AIAA JOURNAL
Vol. 48, No. 12, December 2010

High-Order Numerical Method for Magnetohydrodynamic Control of Shock-Induced Separation

John A. Ekaterinaris*
University of Patras, 265 04 Rio, Greece

DOI: 10.2514/1.45526

Magnetic fields significantly affect the flow of ionized gases and may be exploited for the control of separation, transition, and turbulence. The wave structure of ionized gas high-speed flows under the influence of magnetic fields is more involved than the waves of ordinary gas dynamics and high-resolution is required to accurately compute the complex wave interactions of such flows with discontinuities. Numerical solutions of the nonlinear ideal and viscous magnetohydrodynamic equations are obtained with a high-order-accurate shock-capturing scheme. The numerical method is tested for flows containing strong magnetohydrodynamic discontinuities and smooth flow features to ensure that it maintains high-order accuracy for the smooth parts of the flow, it preserves numerical stability, and eliminates nonphysical features that result from the violation of the divergence-free condition for the magnetic field. Problems with exact solutions, such as the convection of smooth waves caused by magnetic fields, are also solved numerically to validate the method. The numerical method is applied to simulate separation control at the interaction region of an oblique shock with a laminar boundary layer under the influence of magnetic fields.

Nomenclature

Al	=	Alfven number, $\sqrt{V_{Al}/V_{\text{ref}}}$
$\mathbf{B}$	=	magnetic induction vector
B_x, B_y, B_z	=	magnetic vector components
C	=	acoustic speed
C_{Al}	=	Alfven wave speed, $\sqrt{\mathbf{B}\cdot\mathbf{B}/\rho}$
C_f	=	fast wave speed
C_s	=	slow wave speed
$\mathbf{D}$	=	electric displacement vector
$\mathbf{E}$	=	electric field vector
$\mathbf{F^i}$	=	inviscid flux vector
$\mathbf{F^v}$	=	viscous flux vector
$\mathbf{H}$	=	magnetic field vector
Re_b	=	magnetic force number, $B_\infty^2/U_\infty^2\rho_\infty\mu_{m\infty}$
Re_v	=	viscous Reynolds number $\rho_\infty U_\infty L/\mu_\infty$
Re_m	=	magnetic Reynolds number, $U_\infty L\mu_{m\infty}\sigma_\infty$
Re_{Lv}	=	viscous Lundquist number, $\rho_o V_{Al} L_o/\mu$
Re_{Lm}	=	magnetic Lundquist number, $\rho_o V_{Al} L_o/\eta$
u, v, w	=	velocity components
$\mathbf{v}$	=	velocity vector
γ	=	gas constant
ϵ_e	=	dielectric constant
η	=	magnetic resistivity
κ	=	thermal conductivity
μ	=	viscosity
μ_m	=	magnetic permeability
σ	=	electric conductivity

Subscripts

f	=	fast
m	=	magnetic
s	=	slow
x, y, z	=	Cartesian components
ξ, η, ζ	=	curvilienear components

Superscripts

i	=	inviscid fluxes
v	=	viscous fluxes

Presented as Paper 2009-4151 at the 19th AIAA Computational Fluid Dynamics Conference, San Antonio, TX, 22–25 June 2009; received 18 May 2009; revision received 2 February 2010; accepted for publication 10 August 2010.

*Professor, School of Mechanical and Aerospace Engineering, and FORTH/IACM; ekaterin@iacm.forth.gr. Associate Fellow AIAA.

I. Introduction

DURING the past years significant emphasis was given to the development of novel flow control techniques targeting to offer enhanced performance of aircraft and propulsive systems for a wide range of speeds. These techniques reached a high level of sophistication and it is now expected that additional performance can only be achieved by introducing new physical mechanisms for flow control. The exploitation of the interaction between moving electrically conducting gas and magnetic field is an attractive candidate for enhanced flow control authority. The profound influence of electric and magnetic fields on conducting liquids and gases is known for many years. Early investigations [1–3] demonstrated that under the influence of appropriate magnetic fields the shock standoff distance of high-speed flow past blunt bodies increases and the heat transfer rate reduces. The modification of the velocity distribution of wall bounded flows (Hartmann layer) caused by the influence of magnetic fields is well known and attempts were made to use it in industrial applications. The idea of magnetohydrodynamic (MHD) flow control is not also new and attracted the attention of early investigations [4].

Investigation of the dynamics of ionized gases started in the beginning of the last century with the works of Larmor and Alfvén. In 1928, Langmuir [5] coined the term plasma to denote a collection of ions and electrons of the ionized gas produced in discharge tubes. There exists currently a renewed interest for plasma [6] in a wide range of emerging technologies and new applications such as semiconductor processing, electromagnetic pulse devices, nuclear technology, plasma thrusters for space propulsion, plasma induced drag reduction in high-speed flight, and electromagnetic control of flow separation transition and turbulence for conducting fluids. The flow of plasma in the presence of a magnetic field can be described by the system of MHD equations. These equations represent coupling of the fluid dynamical equations with the Maxwell's equations through the addition of Lorentz force and work in the momentum and energy equations. The derivation of the ideal MHD equations, where electrostatic forces, displacement currents, viscosity resistivity, and

heat conduction are neglected and a single vector equation is used for the magnetic induction can be found in textbooks [7–10]. The ideal MHD equations can be extended to the set of equations including viscous effects [10–12]. The numerical methods for the ideal MHD equations [11–13] are based on the techniques developed for gas dynamics. For problems in which the magnetic Reynolds number is very small, the induced magnetic field is negligible and a simplified set of equations including the electromagnetic forces as source terms in the Navier–Stokes equations can be used. Numerical simulations for low magnetics Reynolds number can be obtained [14] with minor modification of a compressible flow solver.

For cases where both electric and magnetic fields are important, the unsteady compressible flow equations containing electromagnetic stress, work, and heat as source terms must be coupled the full Maxwell equations the Faraday's induction law ($\mathbf{B}_t = \nabla \times \mathbf{E}$,), and the generalized Ampere's law ($\mathbf{E_t} = (\nabla \times \mathbf{B}/\mu_m - \mathbf{j}_d)/\epsilon_e$, where $\mathbf{j}_d$ is the current density). For harmonic electromagnetic fields, the constitutive laws for magnetic induction and electric displacement are automatically satisfied. A complete derivation of the equations that couple the full Maxwell equations with the compressible flow equations is given in the literature [10,15]. The numerical treatment of the full MHD equations requires the solution of the full Maxwell equations. A numerical method for flow simulations with strong electric and magnetic fields based on Giordano's formulation [15] was recently presented [16] and applied for the control of high-speed flows.

The ideal MHD equations describe many astrophysical plasmas such as stellar atmospheres and winds, accretion discs, and jets characterized by complex time-dependent flows with strong shocks and current sheets coupled with distributed nonlinear waves. For these astrophysical flows, second-order in space and time schemes have been developed [13,17–21]. The governing equations describing both sparse and dense plasma flows that are relevant in many applications of current interest are the viscous MHD, or the nonideal magnetogasdynamics equations. Viscous MHD flows include coherent sharp field structures often embedded in a turbulent background and second-order accuracy is no longer sufficient to properly resolve small-scale motions and perform long-time integration of wave propagation phenomena in viscous plasma flows. Therefore, there are compelling reasons to develop high-order-accurate schemes for viscous compressible MHD flows. A high-resolution shock-capturing numerical method for the viscous MHD equations is presented in this paper. The distinct characteristics of the present method compared with recent numerical works for the ideal and viscous MHD equations presented in the literature [11–13] are the ability to obtain high-order numerical solutions in complex domains, the computational efficiency for multidimensional numerical solutions, and good shock-capturing capability.

It is well known that application of algorithms, which fail to satisfy the divergence-free condition numerically, can lead to serious defects [22,23]. Usual nonphysical effects that arise when the constraint $\nabla \cdot \mathbf{B} = 0$ is not satisfied is acceleration of the plasma parallel to field lines and plasma transport orthogonal to the magnetic field. The cause of these effects is that violation of the divergence-free constraint results in the addition of source terms in the momentum and energy equations. A numerical scheme that satisfies the divergence-free condition of the Maxwell equations was presented for the first time by Yee [24]. Balsara and Spiecer [25] and Balsara [26] pioneered the design of numerical methods that satisfy the divergence-free condition, which does not appear explicitly in the MHD equations.

Other attempts, which have been made in the literature to enforce explicitly the divergence-free condition, are briefly reviewed. These techniques are also known as divergence-cleaning techniques in the context of MHD equations. Divergence correction can be achieved by projection, which is based on Hodge decomposition, as was first suggested by Brackbill and Barnes [23] in the context of MHD. The numerical magnetic field $\mathbf{B}$ is projected into a zero divergence vector space and the projected $\mathbf{B}$ field is used in the next time step. To implement this approach a Poisson equation needs to be solved. Another method is Powell's source term formulation [27], which is derived from the physical laws if the conditions $\nabla \cdot \mathbf{B} = 0$ is not explicitly used. Source terms proportional to $\nabla \cdot \mathbf{B}$ are added to the equations. The addition of these terms makes the system well behaved but nonconservative. With this method, the divergence errors could be transported to the domain boundaries with certain speed and damped at the same time. Another approach, often referred to as constrained transport methods, was first brought up by Yee [24] in electromagnetics and then adapted to MHD equations thought the use of staggered mesh and a suitably defined discrete approximation so that the divergence of the solution can be maintained zero. This approach has been further developed by combining it with the higher-order Godunov type schemes by Dai and Woodward [19], and by Balsara and Spiecer [25]. Furthermore, Balsara [26] developed such divergence-free reconstruction strategy in an adaptive mesh setting. Toth [21] compared some of the methods mentioned above and introduced the field/flux-interpolated central difference approach, in which no staggered mesh is needed.

In the present work, the Powell source term formulation [27,28] is used for both inviscid and viscous flow numerical solutions. The discretization of the nonlinear convective terms is obtained with high-order finite difference WENO schemes and the viscous terms are discretized using explicit, forth order, centered finite difference formulas. Time marching is performed with explicit Runge–Kutta methods. The numerical method is validated for MHD shock tube problems, the convection and diffusion of magnetic fields for problems with exact solutions, and for the Orszag–Tang [29] (O-T) vortex problem. The method is applied for the simulation of the control of separation of a supersonic, laminar boundary induced by an oblique shock. The rest of this paper is organized as follows. In Sec. II, the governing equations are presented. The eigenvalues and eigenvectors of the inviscid, conservative MHD flux Jacobians were derived for generalized coordinates. These are required in the implementation of the numerical scheme that is outlined in Sec. III. Validation tests and flow control results are presented in Sec. IV.

II. Governing Equations

The governing equations for magnetogasdynamics are obtained by coupling a simplified form of the Maxwell equations, known as *pre-Maxwell* equations, with the Navier–Stokes equations. The pre-Maxwell equations result from the complete set of the Maxwell's equations under the assumption that $\epsilon\omega/\sigma << 1$, where ϵ is the dielectric constant that relates the electric field vector $\mathbf{E}$ with the electric displacement vector $\mathbf{D} = \epsilon\mathbf{E}$, ω is a representative frequency of interest, and σ is the electrical conductivity relating the magnetic induction vector $\mathbf{B}$ with electric $\mathbf{E}$ field vector thought the Ohms's law constitutive relation $\mathbf{j} = \sigma(\mathbf{E} + \mathbf{v} \times \mathbf{B})$, where $\mathbf{v}$ is the velocity of the conducting gas. Therefore, when the time scale of the phenomenon of interest is shorter than the frequency of the plasma Ampere's law reduces to the curl of the magnetic field intensity $\mathbf{H}$ and Ohm's law is an excellent approximation. The system of the Maxwell equations is further complemented with the additional constitutive relation $\mathbf{B} = \mu_m\mathbf{H}$ relating the magnetic field vector $\mathbf{H}$ with the magnetic induction vector. The coupling of the pre-Maxwell equations with the compressible flow equations is carried out thought the momentum and energy equations. The momentum equation is augmented with the extra electromagnetic body force term $F_{\text{em}} = \mathbf{j} \times \mathbf{B}$ while the energy equation is modified by the addition of the electromagnetic energy term $E_{\text{em}} = \mathbf{E} \cdot \mathbf{j}$. The system of magetogasdynamics or MHD is completed with the solution of the induction equation that describes the evolution of the magnetic induction vector. This equation is obtained by eliminating $\mathbf{E}$ from Ohm's law and Faraday's law, ($\nabla \times \mathbf{E} = \partial\mathbf{B}/\partial t$). Subsequently using the pre-Maxwell form of Ampere's law, $\mu_m \nabla \times \mathbf{B} = \mathbf{j}$ (where the time derivative of the electric displacement vector, or the displacement current, has been neglected) the current $\mathbf{j}$ can be eliminated.

The resulting inviscid compressible MHD system in conservation law form is:

$$\frac{\partial}{\partial t}\begin{Bmatrix}\rho\\ \rho u\\ \rho v\\ \rho w\\ e\\ B_x\\ B_y\\ B_z\end{Bmatrix}+\nabla\cdot\begin{bmatrix}\rho\mathbf{v}\\ \rho\mathbf{v}\mathbf{v}^T+(p+|\mathbf{B}|^2/2)\mathbf{I}-\mathbf{B}\mathbf{B}^T\\ \mathbf{v}(e+p+|\mathbf{B}|^2/2)-\mathbf{B}(\mathbf{v}^T\mathbf{B})\\ \mathbf{v}^T\mathbf{B}-\mathbf{B}\mathbf{v}^T\end{bmatrix}=0$$

$$\nabla\cdot\mathbf{B}=0 \tag{1}$$

This form of the governing equations is equivalent with the form shown by Gaitonde [11] if each component of the magnetic induction vector is substituted by $B_j=\hat{B}_j\sqrt{R_b/\mu_m}$, where $R_b=B_\infty^2/U_\infty^2\rho_\infty\mu_{m_\infty}$ is the magnetic force (or pressure) number.

The ideal MHD conservative equations are a system of nonstrictly hyperbolic conservation laws. In addition, the divergence-free condition for the magnetic field must be satisfied at each time step. Inclusion of the divergence-free condition $\nabla\cdot\mathbf{B}=0$ in an explicit form causes difficulties in the numerical implementation. However, Powell [27] and Powell et al. [28] have shown that an *almost* equivalent nonconservative (symmetrizable) MHD system can be derived. The numerical solution of the symmetrizable MHD system does not require to explicitly enforce the divergence-free condition $\nabla\cdot\mathbf{B}=0$ for the magnetic field at each time step (via the solution of a Poisson equation for example), it yields a better conditioned eigensystem and greatly facilitates the application of high-resolution shock-capturing schemes. The divergence-free constraint for the numerical solution of the symmetrizable system is not satisfied exactly but the divergence of the magnetic field converges to zero as the time step and the grid resolution approach to zero. Numerical discretizations of the MHD system introduce other difficulties, for example Toth [21] proved that it is not possible to design a scheme that satisfies both conservation of momentum and the requirement that the discrete acceleration of the Lorentz force is exactly perpendicular to the magnetic field. Taking into account these considerations it appears that Powell's approach is satisfactory because since none of the numerical values agrees exactly with the analytical solution there is no compelling reason to insist that a specific combination of them, namely $\nabla\cdot\mathbf{B}$, should be equal to the analytic value. The right hand side of the symmetrizable inviscid MHD system is identical with the system conservative MHD of Eq. (1) and the left had side contains the ad hoc added nonconservative [27,28] source terms $\mathbf{S}=\nabla\cdot\mathbf{B}[0,\ B_x,\ B_y,\ B_z,\mathbf{v}^T\mathbf{B},u,v,w]^T=\nabla\cdot\mathbf{B}[0,\ (\mathbf{B})_S,\ (\mathbf{v}^T\mathbf{B})_S,\ (\mathbf{v})_S]$. The source terms are retained for the viscous MHD equations which in flux vector form are:

$$\frac{\partial\mathbf{U}}{\partial t}+\frac{\partial\mathbf{F}_x^i}{\partial x}+\frac{\partial\mathbf{F}_y^i}{\partial y}+\frac{\partial\mathbf{F}_z^i}{\partial z}=\frac{\partial\mathbf{F}_x^v}{\partial x}+\frac{\partial\mathbf{F}_y^v}{\partial y}+\frac{\partial\mathbf{F}_z^v}{\partial z}+\mathbf{S} \tag{2}$$

Table 1 Variables and parameters of the compressible MHD equations

Variable/ paramater	Definition	Name
$\rho(\mathbf{x},t)$		Density
$\mathbf{v}(\mathbf{x},t)$	$=(u,v,w)(\mathbf{x},t)$	Velocity vector
$\mathbf{B}(\mathbf{x},t)$	$=(B_x,B_y,B_z)(\mathbf{x},t)$	Magnetic field vector
e	$=\frac{p}{\gamma-1}+\frac{1}{2}(\rho\lvert\mathbf{v}^2\rvert+\lvert\mathbf{B}^2\rvert)$	Total energy
p	$=(\gamma-1)(e-\frac{1}{2}(\rho\lvert\mathbf{v}^2\rvert+\lvert\mathbf{B}^2\rvert)$	Hydrodynamic pressure
$\bar{p}$	$=p+\frac{1}{2}\lvert\mathbf{B}^2\rvert$	Hydrodynamic plus magnetic pressure
Pr	$=\frac{c_p\mu}{\kappa}$	Prandtl number
Re_v	$=\frac{\rho_o V_{\text{ref}}^{\kappa}L_o}{\mu}$	Viscous Reynolds number
Re_m	$=\frac{V_{\text{ref}}L_o}{\eta}$	Magnetic Reynolds number

The expanded forms of the inviscid and viscous flux vectors of the compressible viscous MHD system, Eq. (2), in Cartesian coordinates are:

$$\mathbf{F}_x^i=\begin{Bmatrix}\rho u\\ \rho u^2-B_x^2+\bar{p}\\ \rho uv-B_xB_y\\ \rho uv-B_xB_z\\ [(e+\bar{p})u\\ -(\mathbf{v}\cdot\mathbf{B})B_x]\\ 0\\ uB_y-vB_x\\ uB_z-wB_x\end{Bmatrix}$$

$$\mathbf{F}_x^v=\begin{Bmatrix}0\\ \frac{2}{Re_v}\left(\frac{\partial u}{\partial x}-\frac{1}{3}\nabla\cdot\mathbf{v}\right)\\ \frac{1}{Re_v}\left(\frac{\partial u}{\partial y}+\frac{\partial v}{\partial x}\right)\\ \frac{1}{Re_v}\left(\frac{\partial u}{\partial z}+\frac{\partial w}{\partial x}\right)\\ \frac{1}{Re_v}\left(-\frac{2}{3}(\nabla\cdot\mathbf{v})u+\mathbf{v}\cdot\nabla u+\frac{1}{2}\frac{\partial\mathbf{v}^2}{\partial x}+\frac{1}{Pr}\frac{\partial\mathbf{T}}{\partial x}\right)\\ +\frac{1}{Re_m}\left(\frac{1}{2}\frac{\partial|\mathbf{B}^2|}{\partial x}-\mathbf{B}\cdot\nabla B_x\right)\\ 0\\ \frac{1}{Re_m}\left(\frac{\partial B_y}{\partial x}-\frac{\partial B_x}{\partial y}\right)\\ \frac{1}{Re_m}\left(\frac{\partial B_z}{\partial x}-\frac{\partial B_x}{\partial z}\right)\end{Bmatrix}$$

The state variables and the main parameters of the compressible, viscous MHD system are summarized in Table 1.

The reference speed in the definition of the viscous and magnetic Reynolds number can be the Alfvén wave speed, then these parameters are known as the viscous and resistive Lundquist numbers, respectively.

The Cartesian form of the governing equations is extended to curvilinear coordinates by introducing the transformations $x=x(\xi,\eta,\zeta)$, $y=y(\xi,\eta,\zeta)$, $z=z(\xi,\eta,\zeta)$. The curvilinear coordinate formulation of the inviscid and viscous flux vectors are:

$$\mathbf{F}_\xi^i=\frac{1}{J}\begin{Bmatrix}\rho\tilde{U}\\ \rho\tilde{U}u-\tilde{B}B_x+\xi_x\bar{p}\\ \rho\tilde{U}v-\tilde{B}B_y+\xi_y\bar{p}\\ \rho\tilde{U}w-\tilde{B}B_z+\xi_z\bar{p}\\ [(e+\bar{p})\tilde{U}-\tilde{B}(\mathbf{v}\cdot\mathbf{B})]\\ \tilde{U}B_y-\tilde{B}u\\ \tilde{U}B_y-\tilde{B}v\\ \tilde{U}B_z-\tilde{B}w\end{Bmatrix}$$

$$\mathbf{F}_\xi^v=\frac{1}{J}\begin{Bmatrix}0\\ \frac{1}{Re_v}(\xi_x\tau_{xx}+\xi_y\tau_{xy}+\xi_z\tau_{xz})\\ \frac{1}{Re_v}(\xi_x\tau_{xy}+\xi_y\tau_{yy}+\xi_z\tau_{yz})\\ \frac{1}{Re_v}(\xi_x\tau_{xz}+\xi_y\tau_{yz}+\xi_z\tau_{zz})\\ \frac{1}{Re_v}(\xi_xE_x+\xi_yE_y+\xi_zE_z)\\ +\frac{1}{Re_m}(\xi_xM_x+\xi_yM_y+\xi_zM_z)\\ \frac{1}{Re_m}(\xi_xB_{xx}+\xi_yB_{xy}+\xi_zB_{xz})\\ \frac{1}{Re_m}(\xi_xB_{xy}+\xi_yB_{yy}+\xi_zB_{yz})\\ \frac{1}{Re_m}(\xi_xB_{xz}+\xi_yB_{yz}+\xi_zB_{zz})\end{Bmatrix}$$

where

$$\tau_{xx} = -\frac{2}{3}\mu\nabla\cdot\mathbf{v} + 2\mu u_x$$

$$\tau_{xy} = \mu(u_y + v_x)\tau_{yy} = -\frac{2}{3}\mu\nabla\cdot\mathbf{v} + 2\mu v_y$$

$$\tau_{xz} = \mu(u_z + w_x)\tau_{zz} = -\frac{2}{3}\mu\nabla\cdot\mathbf{v} + 2\mu w_z \qquad \tau_{yz} = \mu(v_z + w_y)$$

$$E_x = u\tau_{xx} + v\tau_{xy} + w\tau_{xz} + \frac{\mu\gamma}{Pr}(\xi_x e_\xi + \eta_x e_\eta + \zeta_x e_\zeta)$$
$$E_y = u\tau_{xy} + v\tau_{yy} + w\tau_{yz} + \frac{\mu\gamma}{Pr}(\xi_y e_\xi + \eta_y e_\eta + \zeta_y e_\zeta)$$
$$E_z = u\tau_{xz} + v\tau_{yz} + w\tau_{zz} + \frac{\mu\gamma}{Pr}(\xi_z e_\xi + \eta_z e_\eta + \zeta_z e_\zeta)$$

$$M_x = 0.5|B|_x^2 - (B_x B_{x,x} + B_y B_{x,y} + B_z B_{x,z})$$
$$M_y = 0.5|B|_y^2 - (B_x B_{y,x} + B_y B_{y,y} + B_z B_{y,z})$$
$$M_z = 0.5|B|_z^2 - (B_x B_{z,x} + B_y B_{z,y} + B_z B_{z,z})$$

$$B_{xx} = 0, \qquad B_{xy} = B_{y,x} - B_{x,y}, \qquad B_{xz} = B_{z,x} - B_{x,z}$$
$$B_{yx} = B_{x,y} - B_{y,x}, \qquad B_{yy} = 0, \qquad B_{yz} = B_{z,y} - B_{y,z}$$
$$B_{zx} = B_{x,z} - B_{z,x}, \qquad B_{zy} = B_{y,z} - B_{z,y}, \qquad B_{zz} = 0$$

and $\tilde{U}$ and $\tilde{B}$ are the contravariant velocity and magnetic induction vectors along the ξ direction defined as $\tilde{U} = u\xi_x + v\xi_y + w\xi_z$, $\tilde{B} = B_x\xi_x + B_y\xi_y + B_z\xi_z$, J is the Jacobian of the transformation, and ξ_x, ξ_y, ξ_z are metric terms.

The symmetrizable form of the equations for ideal [30] and viscous [12] MHD has been recently used with different numerical techniques to make possible the enforcement of the divergence-free condition that appears explicitly in the conservative form. Similar to other modern shock-capturing methods, weighted essentially non-oscillatory (WENO) uses local characteristic decomposition for the evaluation of the numerical flux where the conservative fluxes are separated into families of waves. Considerable work is required to evaluate the MHD eigensystem. There are seven waves in the MHD system. In addition to the entropy wave, which propagates with the fluid speed, **v**, there are three additional wave modes, which can propagate with different speeds. According to the magnitude of the wave speeds, these three modes are called fast, intermediate (Alfvén), and slow waves. The Alfvén slow and fast waves degenerate into acoustic waves when the magnetic induction vector vanishes ($\mathbf{B} = 0$) and a spike in the numerical results of the shock tube appears as a compound wave [6,13], as is shown in the numerical results. The fast and slow waves are compressive, while the intermediate Alfvén wave is not. Depending on the direction and the magnitude of the magnetic field, these wave speeds may coincide. Thus the MHD equations form a nonstrictly hyperbolic system. In spite of this, a complete set of eigenvectors can be found, and with proper normalization, they are well defined [28,30,31]. In this work, the 3-D extension of the Yee and Sjogreen [30] and Cargo and Gallice [32] eigenvectors for the nonconservative MHD system is used.

III. Numerical Scheme

Finite difference WENO discretization of the conservative form of the ideal MHD equations has been presented by Jiang and Wu [33] In the present work, the inviscid fluxes of the symmetrizable system are evaluated with the standard, conservative finite difference WENO schemes [34,35]. The derivatives of the inviscid fluxes are computed as

$$\frac{\partial f}{\partial x} = \frac{\hat{f}_{i+1/2} - \hat{f}_{i-1/2}}{\Delta x} \tag{3}$$

where $\hat{f}_{i+1/2}$ denotes the numerical flux which is reconstructed using high-order accuracy. The increase of the order of accuracy of WENO implies increase the stencil width. The stencil width for the fifth, seventh, and ninth accurate WENO schemes is 7, 9, and 11, respectively. WENO reconstruction of the left and right states U_L, U_R about $i-1/2$ and $i+1/2$, respectively, is carried out on the characteristic space. Formulas for reconstruction with (fifth or higher order of accuracy (seventh, and ninth), and Runge–Kutta methods for time marching can be found in [34] and references therein.

For the numerical solution of the three-dimensional symmetrizable (nonconservative) MHD system with the finite difference WENO scheme, it is necessary to define an average state of the left and the right states at an interface. A Roe-type approximate Riemann solver, which is an improvement to the Riemann solvers proposed by Brio and Wu [13] is used. For high-order methods, such as WENO, the choice of the numerical flux does not affect significantly the overall accuracy. Therefore, the computationally efficient Lax–Friedrichs numerical flux is used and the average state $\bar{U}$ is defined for the variables $\mathbf{q} = [\rho, u, v, w, h^*, B_x, B_y, B_z]^T$ where $h^* = (e + p + |\mathbf{B}|^2)/\rho$ using Roe's averaging. Once the average state has been

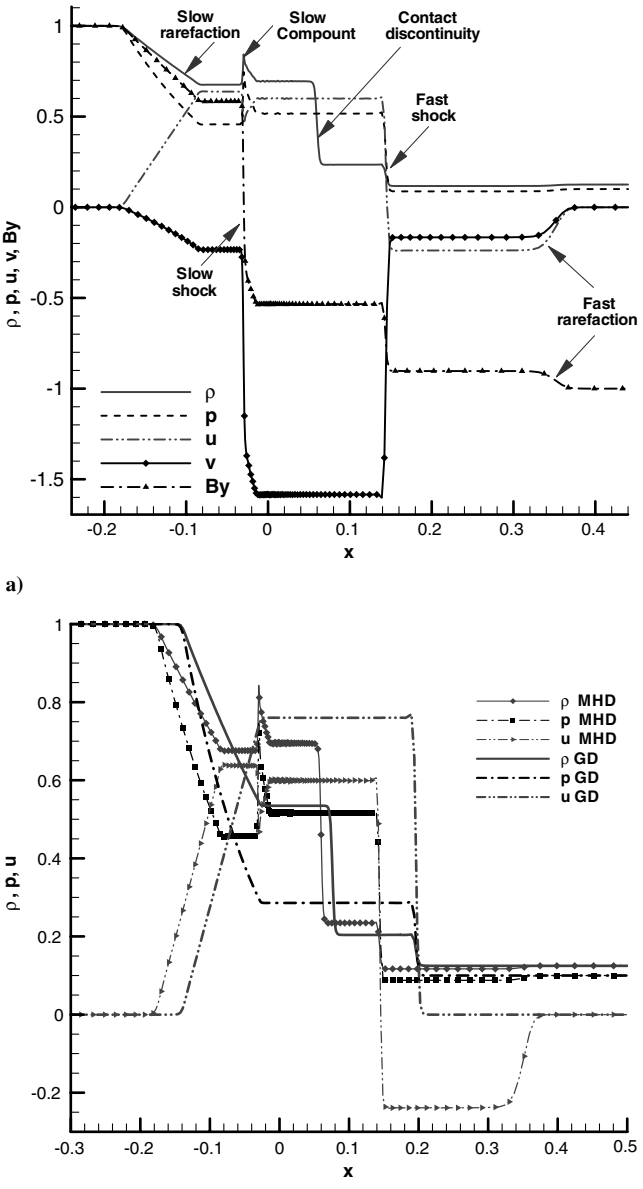

Fig. 1 Schematics of a) wave structure of MHD shock tube problem, and b) comparison with the gas dynamic ($B = 0$) shock tube problem.

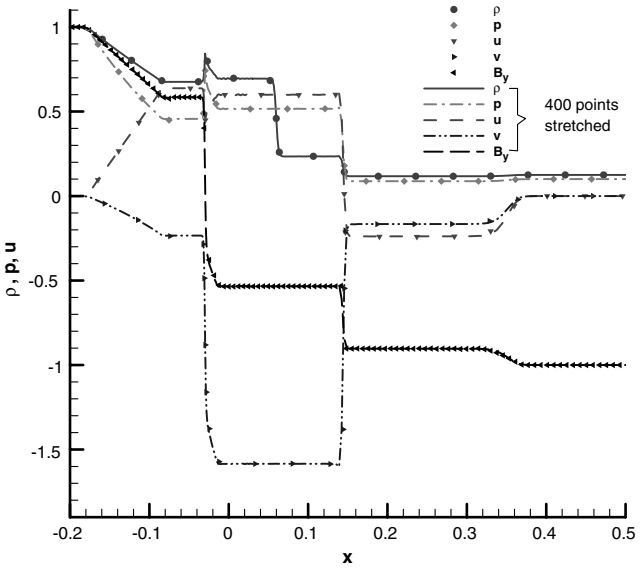

Fig. 2 Effect of grid stretching on the resolution of discontinuities for the MHD shock tube problem.

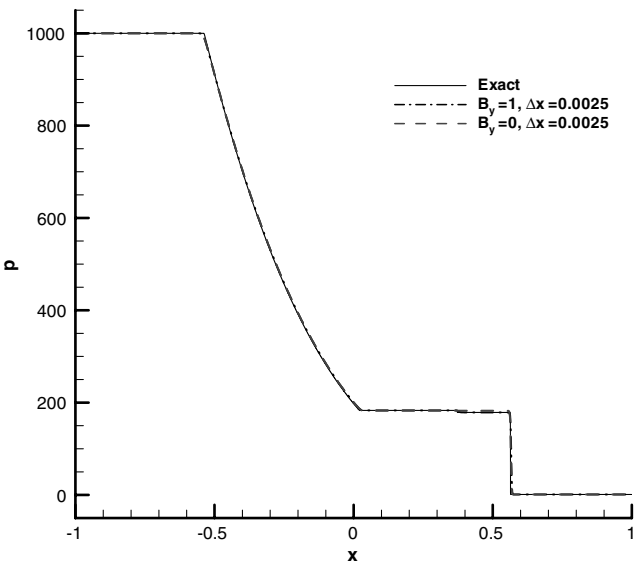

Fig. 4 Effect of the transverse magnetic field component B_y on the formation of pressure discontinuities.

defined the conservative flux vectors are first projected on the characteristic space where the reconstruction is carried out and then the numerical flux is reprojected back to the conservative variables space and the derivatives are computed with Eq. (3). Therefore, evaluation of a proper set of right and left eigenvectors for the conservative flux vectors is a crucial step of the WENO solver.

The eigensystem of Eqs. (1) has been extensively studied. It was pointed out [31] that the set of eigenvectors can become singular at the points where the eigenvalues are degenerate. Brio and Wu [13] have given a proper choice of normalization that avoids these singularities and provides a complete set of eigenvectors. The numerical scheme was tested for the eigenvectors derived by Brio and Wu. For one-dimensional shock tube problems, good solutions were obtained. However, it was found that for multidimensional flows a divergence-cleaning procedure was necessary. The same conclusion was reached by Jiang and Wu [33]. Divergence cleaning could become quite costly for three-dimensional computations. Therefore the symmetrizable form was adopted and the set of eigenvectors given by Cargo and Gallice [32] was used.

IV. Results

Brio and Wu [13] presented one-dimensional solutions for ideal MHD shock tube problems, while Jaiang and Wu [33] using the same formulation (without source term) and divergence cleaning for two-dimensional flows obtained high-order numerical solutions with WENO reconstruction. The source term formulation was first implemented in the finite volume context [27] while Warburton and Karniadakis [12] implemented the same formulation in the high-order discontinuous Galerkin context for flows without discontinuities. High-order finite difference numerical solutions for nonideal MHD flows without discontinuities were obtained by Gaitonde [11]. In this work the source term formulation is adopted and a Riemann solver with WENO reconstruction that is carried out in generalized coordinates is used. Therefore, systematic validation is required before the method is applied to more realistic flow cases. Simple validation shock tube problems suggested by Brio and Wu [13], and exact results for smooth flow problems [11] are used to validate the present method. All numerical solutions are computed with a 3-D code by adding appropriate number of points (depending on the order of the WENO scheme) for one- and two-dimensional problems.

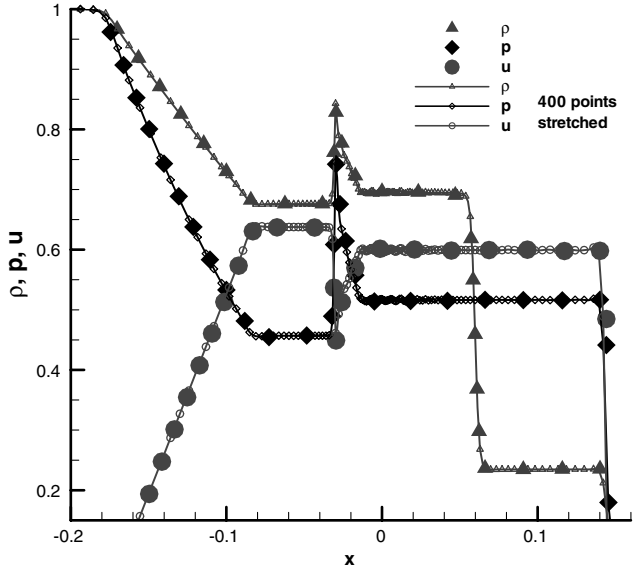

Fig. 3 Detailed comparison of the numerical solution with uniform mesh (symbols) and stretched mesh (lines with symbols).

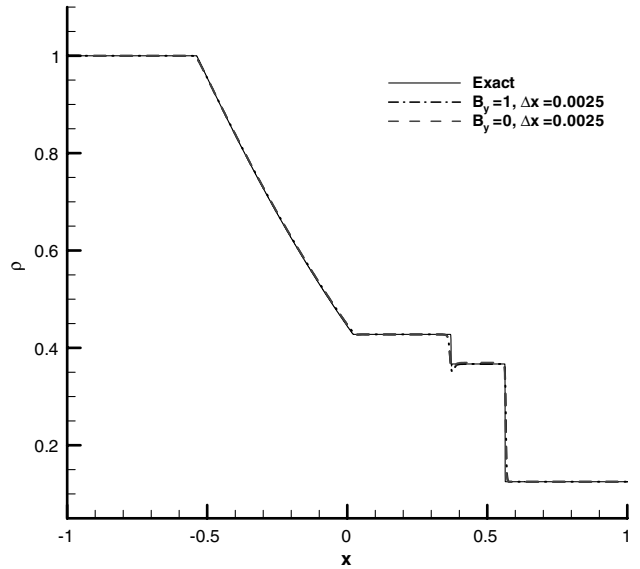

Fig. 5 Effect of the transverse magnetic field component B_y on the formation of density discontinuities.

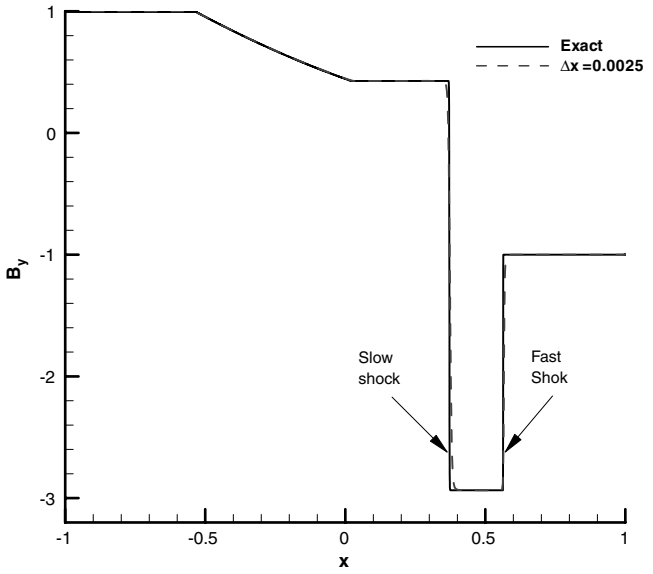

Fig. 6 Computed transverse field B_y.

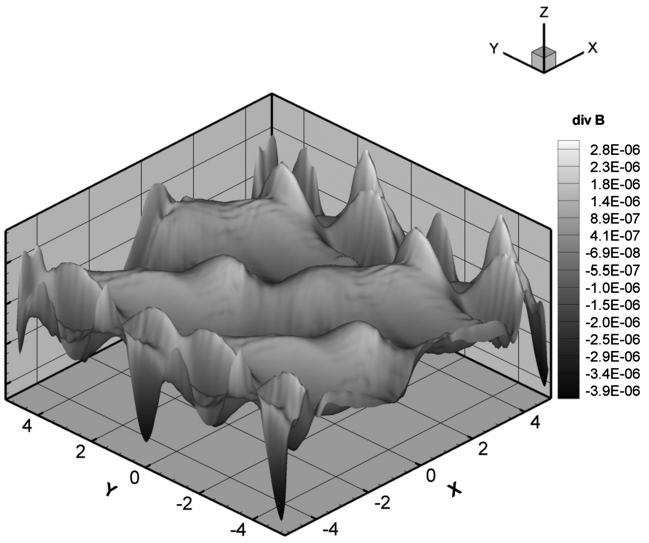

Fig. 9 Computed magnetic field divergence for two-dimensional Alfvén propagation.

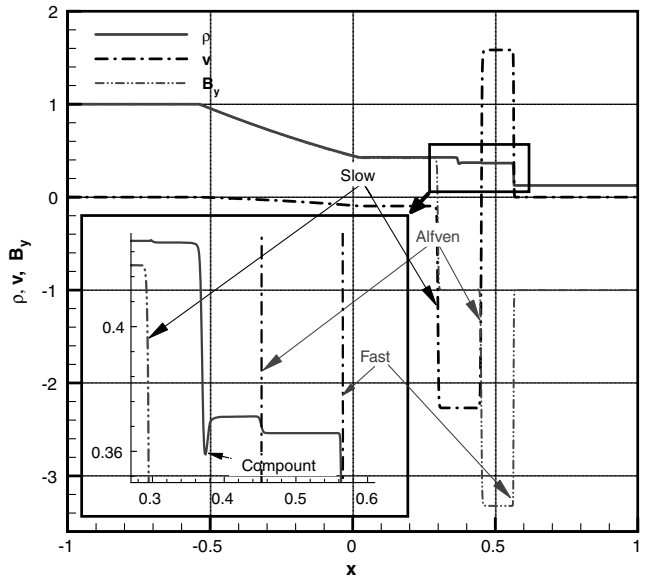

Fig. 7 Generation of intermediate Alfven waves with the addition of a streamwise magnetic field $Bx = 4$.

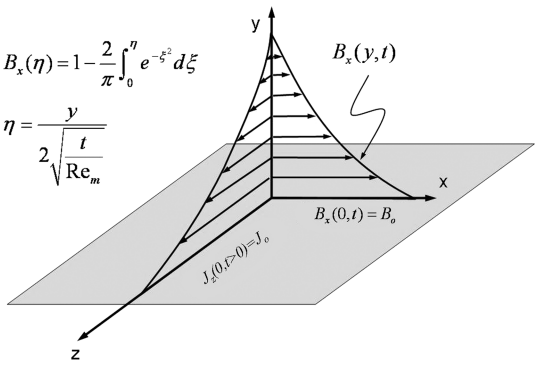

Fig. 10 Schematic of Alfvén diffusion.

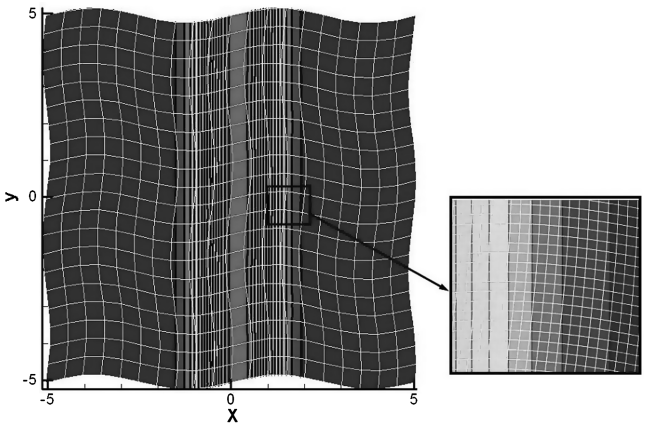

Fig. 8 One-dimensional Alfvén wave propagation computed with a 2-D distorted mesh.

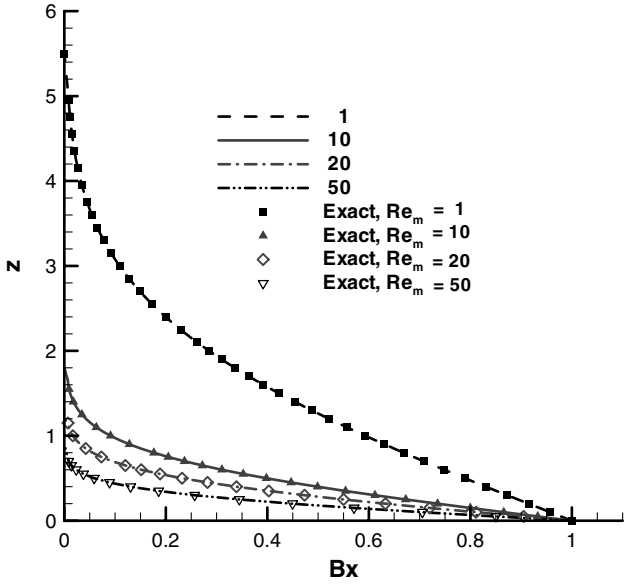

Fig. 11 Comparison with the exact Alfvén diffusion at different magnetic Re_m.

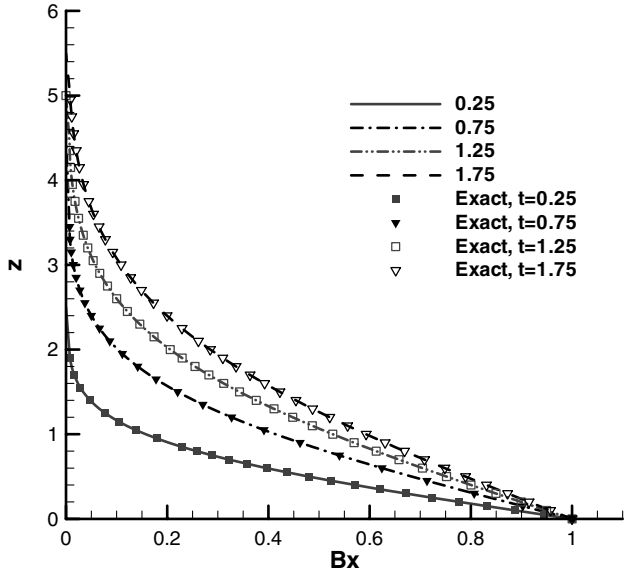

Fig. 12 Comparison with the exact Alfvén diffusion at different times.

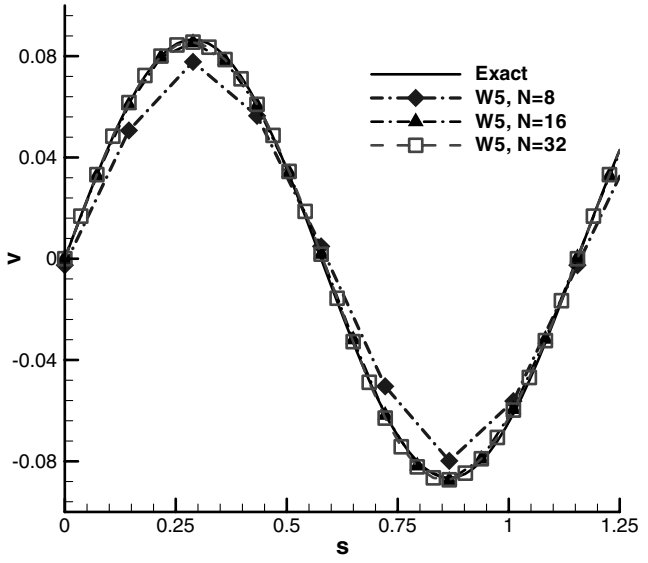

Fig. 13 Comparison with the exact v velocity.

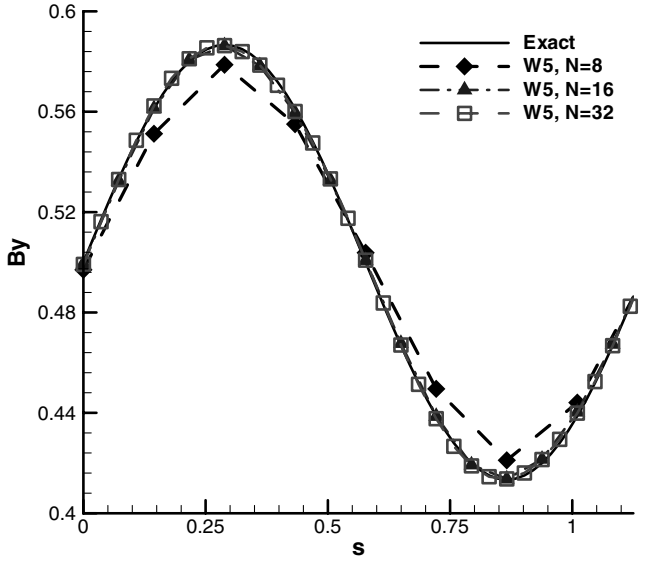

Fig. 14 Comparison with the exact magnetic field component B_y.

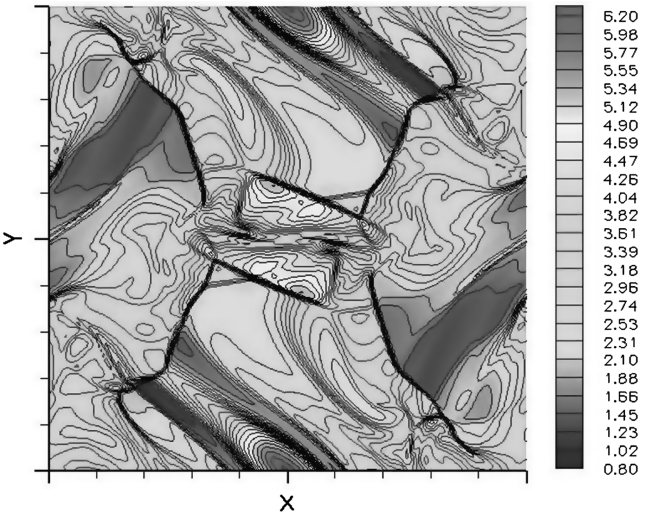

Fig. 15 Computed density field for the O-T vortex at time $t = \pi$ with a 200 × 200 cell mesh.

The first validation case is the coplanar MHD Riemann problem proposed by Brio and Wu [13]. This problem is the MHD analog of the Sod's shock tube (ST) problem for gas dynamics and it is referred to as the ST-MHD-I problem. The interaction for ST-MHD-I occurs under a constant in the x direction magnetic field $B_x = 0.75$ and $\gamma = 2.0$ in the region $-1 \le x \le 1$. The two initial constant left state U_L for $x < 0$ and right state U_R for $x > 0$ of the ST-MHD-I problem that contain discontinuities for the gas dynamics quantities and the y component of the magnetic field and are given by:

$$U_L = [\rho_L, u_L, v_L, p_L, (B_y)_L] = [1.000, 0.0, 0.0, 1.0, +1.0]$$
$$-1 \le x < 0$$
$$U_R = [\rho_R, u_R, v_R, p_R, (B_y)_R] = [0.125, 0.0, 0.0, 0.1, -1.0]$$
$$0 \le x \le 1$$

The computed profiles for density ρ, pressure p, the velocity components u, v, and the B_y component of the magnetic filed vector at time $t = 0.01$ are shown in Figs. 1–3. The wave structure is annotated in Fig. 1a. In Fig. 1b, the solution computed with the same code but without magnetic field is shown with dashed line. It is clear that the imposed magnetic field slows down the shock and reduces the intensity of velocity shocks. On the other hand, the imposed magnetic field increases the pressure jump at the shock location.

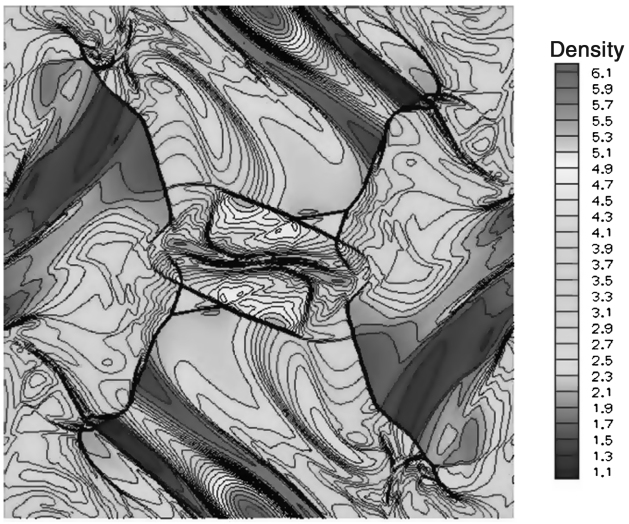

Fig. 16 Computed density field for the O-T vortex at time $t = \pi$ with a 400 × 400 cell mesh.

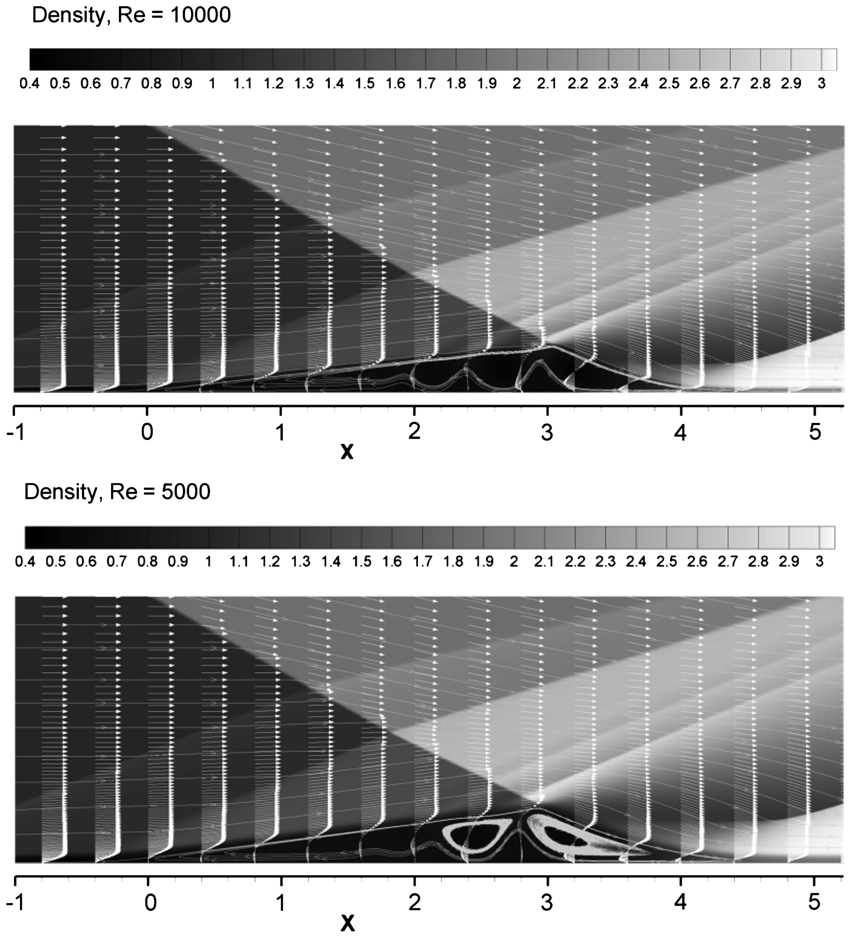

Fig. 17 Computed flowfields at $Re = 5000$ and $Re = 10,000$ for shock laminar boundary layer interaction no control.

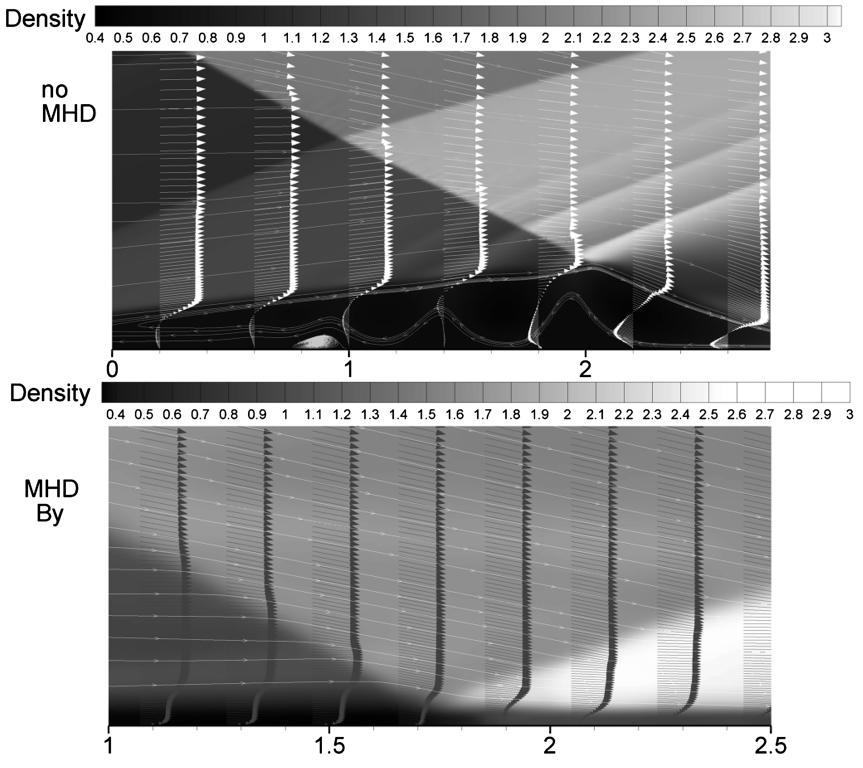

Fig. 18 Separation suppression with B_y.

Numerical solutions were obtained with different grid densities and because the numerical method is suitable for arbitrary meshes a solution was computed with grid stretching. A comparison of a solution computed with very high density (5000 intervals and $\Delta x = 0.0002$ and uniform mesh), and a solution computed with 400 intervals and stretched mesh in the interaction region is shown in Fig. 2. A detailed comparison in the interaction region is shown in Fig. 3. In both figures only few symbols of the high density mesh are show. Clearly the solution computed on the stretched mesh provides the same resolution as the very fine mesh.

The second validation Riemann problem is the shock tube problem proposed by Brio and Wu [13] to demonstrate the robustness of their scheme for high Mach number flows caused by large pressure ratio of the left and right states. This problem is referred to as ST-MHD-II, and the only difference with the ST-MHD-I problem is that the pressure ratio instead of 10 is 10^4 ($p_L = 1000$) and there is no uniform magnetic field along the x direction ($B_x = 0.0$). This problem is solved until final time $t = 0.012$. The computed solutions for the ST-MHD-II problem are shown in Figs. 4–7. In Figs. 4 and 5 the effect of the transverse B_y magnetic field component on the development of pressure and density discontinuities is shown. The slow and fast shock waves induced by $B_y = \pm 1$ are indicated in Figs. 4 and 6. The large pressure ratio results in a high-speed shock. Addition of a uniform magnetic field along the x direction for the original ST-MHD-II problem further alters the wave structure. The generation of intermediate Alfvén waves, when an additional magnetic field component $B_x = 4.0$ was imposed, is shown in Fig. 7.

The first one-dimensional validation example with an analytic solutions that includes only smooth features is Alfvén wave propagation along a line $-5 \le x \le 5$ with periodic ends. The initial conditions for this problem are uniform density $\rho = 1$ and constant total pressure $p + |\mathbf{B}|^2/2$. Under these conditions an initial waveform $B_z(x, 0) = B_0(x)$ propagates with constant wave speed is B_x. A detailed description of this problem is given by Gaitonde [11]. The computed solution at $t = 10$ for initial condition $B_z(x, 0) = e^{-x^2}$ agrees to plotting accuracy with the exact result. A two-dimensional analog of the one-dimensional Alfvén wave propagation with $B_z(x, y, 0) = e^{-x^2}$ was computed on an artificially distorted relatively coarse mesh. The computed magnetic field is shown in Fig. 8. The computed divergence of the magnetic field at the final time is shown in Fig. 9. It appears that for long time integration the constraint $\nabla \cdot \mathbf{B} = 0$ was retained almost to machine zero even for a relatively coarse distorted mesh.

The next one-dimensional validation example, is diffusion of a magnetic field [11]. The initial conditions for the electromagnetic field are shown in the schematic of Fig. 10. At time $t = 0$ a magnetic field of intensity $B_x = B_0$ is considered on the surface of a conductor. This magnetic fields diffuses in the ionized gas and the diffusion length is proportional to the magnetic Reynolds number, Re_m, and the final time. Comparisons of computed solutions with the exact result, $B_x(\eta) = 1 - (2/\pi) \int_0^\eta e^{\xi^2}\, d\xi$, $\eta = 0.5y/\sqrt{t/Re_m}$, are shown in Figs. 11 and 12. The computed solutions for different magnetic Reynolds number Re_m at $t = 1.75$ (see Fig. 11) and for magnetic Reynolds number $Re_m = 1$ at different final times (see Fig. 12) are in good agreement with the exact result. Another essentially one-dimensional example considered was computation of the Hartmann layer. The computed solutions for moderate Reynolds numbers (to avoid very small time steps imposed by the explicit method) were also found in good agreement with the exact result.

A two-dimensional validation example, Alfvén wave propagation in a rectangular periodic domain, was considered next. The numerical solution of this problem [21] is computed in a rectangular domain $0 \le x \le 1/cos(\theta)$, $0 \le y \le 1/cos(\theta)$, $\theta = \pi/6$. The gas constant is $\gamma = 5/3$ and the initial density and pressure are constant $\rho(x, y, t = 0) = 1$, $p(x, y, t = 0) = 0.1$. The initial velocity and magnetic field components parallel to the lines $\theta = \pi/6$ are constant $u_\parallel = 0$, $B_\parallel = 1$, and the normal to these lines components are $u_\perp = B_\perp = 0.1 \sin[2\pi(x \cos\theta + z \sin\theta)]$. Periodic boundary conditions are specified and the solution is computed until final time $t = 10$. Comparisons of the exact solution with numerical solutions computed with different number of intervals $N = 8$, 16, 32 and the fifth-order-accurate WENO-5 scheme are shown in Figs. 13 and 14. The y components of the computed velocity and magnetic field vectors of Fig. 13 and 14, respectively, compare favorably with the exact result. The same agreement is observed for the components along the x direction. The agreement improves with the increase of the number of intervals and the convergence rate of the computed solutions for this problem with smooth data was found to be close to the design order of accuracy of the WENO-5 scheme.

The MHD O-T [29] vortex problem is a classical validation example for ideal MHD shock-capturing methods and has been used by several investigators [12,21,30,36] to demonstrate the resolution of their MHD Riemann solvers. The O-T vortex problem is computed in a square domain $0 \le x \le 2\pi$, $0 \le y \le 2\pi$ for $\gamma = 5/3$, constant initial density, $\rho(x, y, t = 0) = \gamma^2$, and constant pressure, $p = \gamma$. The initial conditions at $t = 0$ for the velocity and the magnetic field components are smooth functions of position specified as follows: $u(x, y) = -\sin(y)$, $v(x, y) = \sin(x)$, $B_x(x, y) = -\sin(y)$, $B_y(x, y) = 2\sin(x)$. The solution is computed with constant time step and periodic boundary conditions until final time $t = \pi$. The numerical solution develops discontinuities in finite solution time, $t \approx \pi/6$,

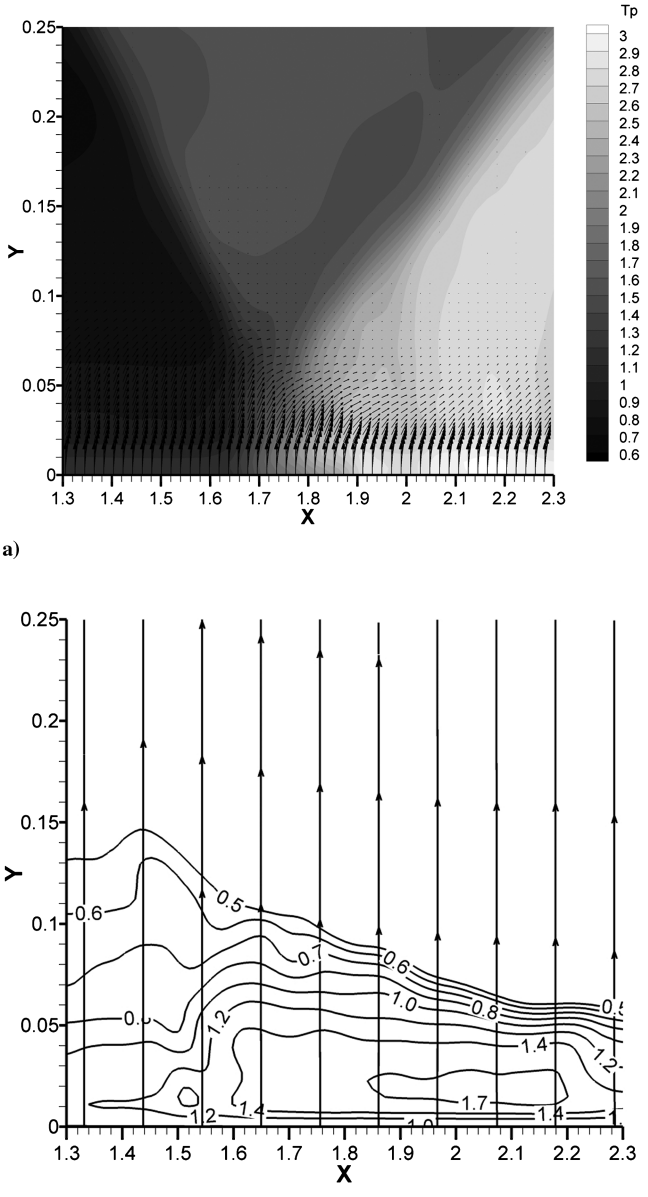

Fig. 19 Magnetic and electric field at the interaction region.

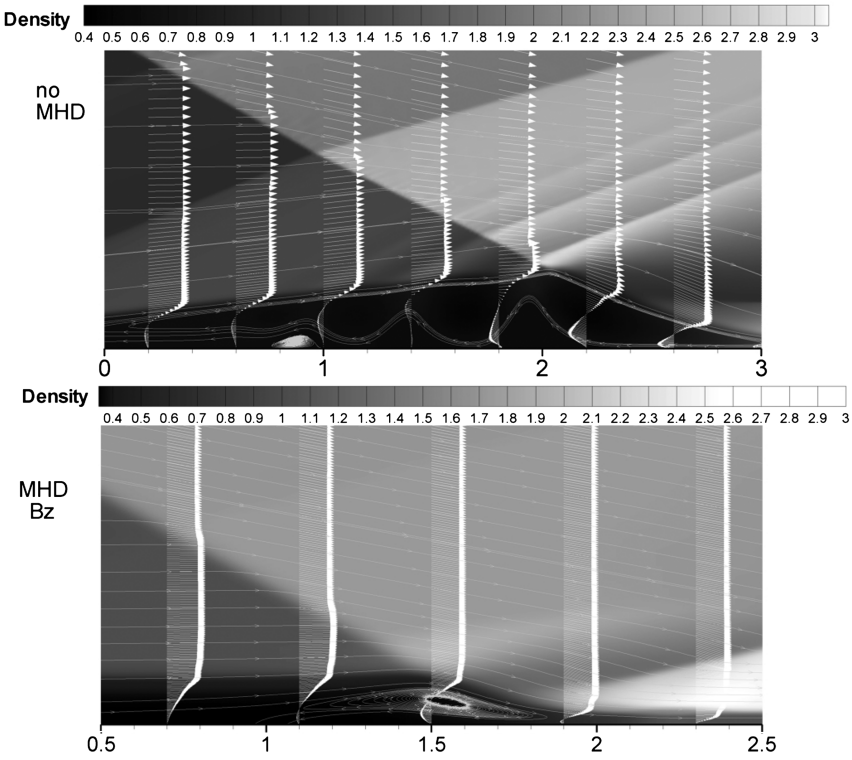

Fig. 20 Separation suppression with B_z.

initially at the periodic boundaries of the computational domain. The discontinuities propagate in the interior and at time $t = \pi$ complex discontinuity patterns are found for all quantities. The computed density field at time $t = \pi$ for a numerical solution computed with a 200×200 cell grid and the WENO-5 scheme is shown in Fig. 15. The general features of this numerical solution are in agreement with the features obtained with a 400×400 cell denser grid shown in Fig. 16. On the denser mesh, finer flow features can be distinguished at the center of the domain. The pressure and temperature fields demonstrate that in addition to sharp shocks exist contact discontinuities. The computed magnetic field (not shown here) is also discontinuous, however, the magnetic field contains coarser structure compared with the density or gas pressure field. The computed temperature field could indicate the location of contact discontinuities [21]. At larger final time $t = 2\pi$, the computed flowfield structures become finer because the O-T vortex was introduced as an example for the study of two-dimensional MHD turbulence.

The favorable comparisons of computed solutions with exact results and standard MHD problems including strong discontinuities for all MHD state variables established the required confidence for the accuracy of the numerical method. The numerical method was then applied for the simulation of flow separation control. The case considered is control of separation induced on a supersonic boundary layer at $M = 3$ by an oblique shock at an angle of $\theta = 30$ deg. Computed solutions of the flow without magnetic field at $Re = 5000$ and $Re = 10000$ per unit length on a mesh with 100 intervals uniformly distributed per unit length and 200 points stretched in the normal directions are shown in Fig. 17. Clearly, the separation bubble that develops ahead of the oblique shock incidence is larger at the lower Reynolds number. Assuming that the gas is ionized and, $Re_v = Re_m = 10^4$ (Hartman number $Ha = \sqrt{Re_v Re_m} = 10^4$) per unit length, control of flow separation by magnetic fields was simulated.

First a magnetic field normal to the flow direction $B_y = 1$ is imposed on the surface of the plate. The oblique shock that is generated by a wedge for $M = 3$ freestream speed and impinges angle $\theta = 30$ is imposed as the boundary condition at the top of the domain from the oblique shock relations for inviscid flow. The flow is supersonic everywhere, and therefore all inflow conditions are specified at the inflow boundary and simple extrapolation is used at the outflow. On the surface the nonslip boundary condition is specified for the velocities and the density and pressure on the wall are extrapolated from the interior assuming that $\partial \rho_w / \partial y = \partial p_w / \partial y = 0$ while $\mathbf{B}_w = (0, 1, 0)$. This surface boundary condition for the magnetic field is an approximation of the magnetic field generated by coils that have their axis along the y direction. The computed flowfields with magnetic field and without magnetic field are compared in Fig. 18. The imposed B_y field on the wall generates a Hartmann-like effect and results in complete flow attachment. The magnetic field vectors and the computed total pressure are plotted in Fig. 19a. The current can be obtained form the computed magnetic induction field as $\mathbf{j} = \nabla \times \mathbf{B}/\mu_{\mathbf{m}}$ and the lines of current with the contours of the magnetic pressure $|\mathbf{B}|$ are shown in Fig. 19b.

Next a magnetic field with a component $B_z = 1$ along the span of the plate was considered for flow control. This case is analogous to the schematic of Fig. 10, where the imposed magnetic field diffuses along the normal to the wall direction and the current along the stream wise direction also diffuses in the normal to the wall direction. It corresponds to a case where the axis of the coils is along the transverse, z, direction. The numerical solution computed on the same mesh, flow and boundary conditions but with $\mathbf{B}_w = (0, 0, 1)$ is shown in Fig. 20. It appears that significant attachment of the flow was achieved. The magnetic field and the computed total pressure in the interaction region for the case with $\mathbf{B}_w = (0, 0, 1)$ is plotted in Fig. 21 and it can be compared with the case $\mathbf{B}_w = (0, 1, 0)$ of Fig. 19. The current vectors along the stream wise direction obtained from the computed magnetic induction field and the contours of the magnetic pressure $|\mathbf{B}|$ are shown in Fig. 21b.

It was found that complete elimination significant reduction of the separated flow region of shock-induced separation can be achieved with appropriate size magnetic fields. The intensity of the magnetic fields required to obtain complete elimination of separation induced by the impingement of a strong oblique shock on a spatially developing laminar boundary layer is quite large. However, the present method can be used for detailed comparisons with experiments and further investigation of the physics of MHD flow control.

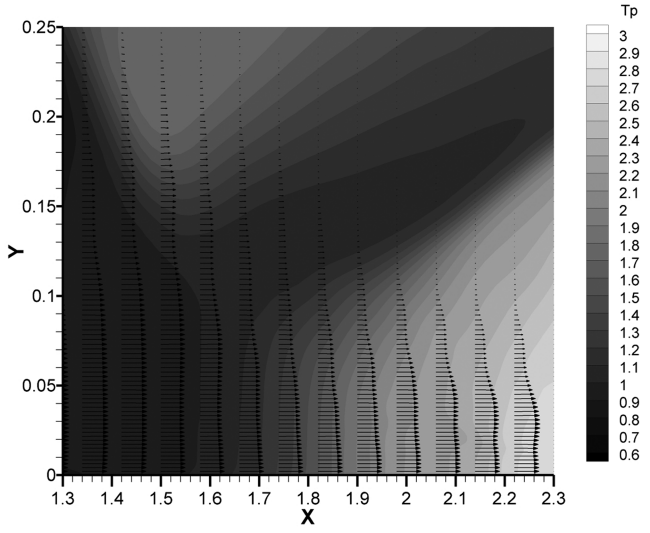

a)

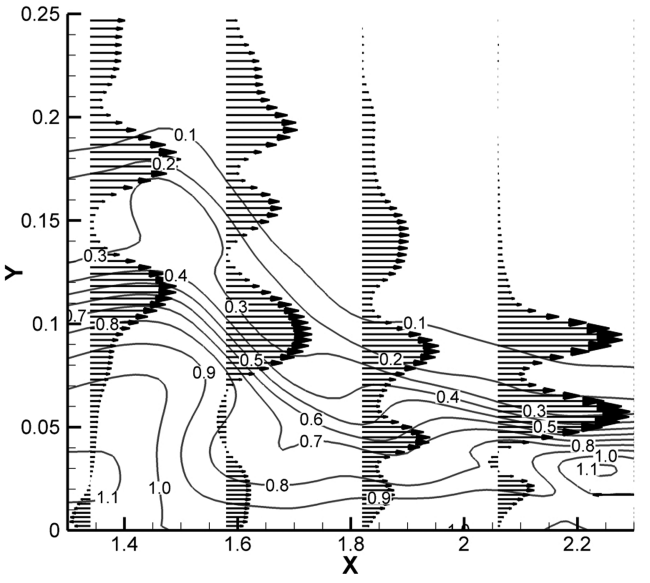

b)

Fig. 21 Magnetic and electric field at the interaction region.

V. Conclusions

A high-order method for ideal and viscous compressible MHD equations has been developed, validated for model problems with exact solutions, and applied for separation control caused by an oblique shock impinging on a laminar boundary layer. The symmetrizable form of the governing equations was used to ensure preservation of the divergence-free constrain for the magnetic field. The inviscid fluxes were discretized using the standard finite difference WENO scheme and the viscous terms were computed with central fourth-order-accurate finite differences. The eigensystem of the MHD equations was derived for arbitrary directions and used for the WENO finite difference scheme that is applied to the generalized coordinates form of the governing equations. The numerical scheme was validated for standard test problems with exact solutions that are available in the literature. It was shown that for smooth flow problems the method achieves the design order of accuracy and provides sharp resolutions of discontinuities. The numerical method was applied for the simulation of flow separation control. It was found that flow separation can be significantly reduced or completely eliminated with the application of appropriate magnetic fields. The numerical method has all the essential ingredients for simulations of complex MHD physics in transition and turbulence control of high-speed flows.

References

[1] Bush, W. B., "Magnetohydroynamic-Hypersonic Flow Past a Blunt Body," *Journal of Aerospace Science*, Vol. 25, No. 11, 1958, pp. 685–690.

[2] Ziemer, R. W., and Bush, W. B., "Magnetic Field Effects on Bow Shock Stand-Off Distance," *Physical Review Letters*, Vol. 1, No. 2, 1958, pp. 58–59. doi:10.1103/PhysRevLett.1.58

[3] Sears, W. R., and Resler, E. L., "Magneto-Aerodynamic Flow Past Bodies," *Advances in Applied Mathematics*, Academic Press Inc., New York, 1964.

[4] Ericson, W. B., and Maciulaitus, A., "Investigation of Magneto-hydroynamic Flow Control," *Journal of Spacecraft and Rockets*, Vol. 1, No. 3, 1964, pp. 283–289. doi:10.2514/3.27637

[5] Langmuir, I., "Oscillations in Ionized Gases," *Proceedings of the National Academy of Sciences of the United States of America*, Vol. 14, No. 8, 1928, pp. 627–637. doi:10.1073/pnas.14.8.627

[6] Shang, J. S., "Recent Research in Magneto-Aerodynamics," *Progress in Aerospace Sciences*, Vol. 37, No. 1, 2001, pp. 1–20. doi:10.1016/S0376-0421(00)00015-4

[7] Sherclieff, J. A., *A Textbook of Magnetohydrodynamics*, Pergamon Press, New York, 1965.

[8] Landau, L. D., and Lifshits, E., *Electrodynamics of Continuous Media*, Pergamon Press, New York, 1960.

[9] Jefrrey, A., *Magnetohydrodynamics*, Oliver and Boyd, London, 1966.

[10] Pai, S. I., *Magnetohydrodynamics and Plasma Dynamics*, Springer–Verlag, New York, 1963.

[11] Gaitonde, D. V., "Higher-Order Solution Procedure for Three-Dimensional Nonideal Magnetogasdynamics," *AIAA Journal*, Vol. 39, No. 11, 2001, pp. 2111–2120. doi:10.2514/2.1207

[12] Warburton, T. C., and Karniadakis, G. E., "A Discontinuous Galerkin Method for the Viscous MHD Equations," *Journal of Computational Physics*, Vol. 152, No. 2, 1999, pp. 608–641. doi:10.1006/jcph.1999.6248

[13] Brio, M., and Wu, C. C., "An Upwind Differencing Scheme for the Equations of Ideal Magnetohydrodynamics," *Journal of Computational Physics*, Vol. 75, No. 2, 1988, pp. 400–422. doi:10.1016/0021-9991(88)90120-9

[14] Poggie, J., and Gaitonde, D. V., "Computational Studies of Magnetic Control in Hypersonic Flow," AIAA Paper 2001-0196, Jan. 2001.

[15] Giordano, D., "Hypersonic Flow Governing Equations with Elacreomagnetic Fields," AIAA Paper 2002-2165, June 2002.

[16] MacCormack, R. W., "Flow Simulation of Aerodynamic Flow Including Induced Magnetic and Electric Fields," AIAA Paper 2008-4010, June 2008.

[17] Dai, W., and Woodward, P. R., "An approximate Riemann Solver for Ideal Magnetohydrodynamics," *Journal of Computational Physics*, Vol. 111, No. 2, 1994, pp. 354–372. doi:10.1006/jcph.1994.1069

[18] Dai, W., and Woodward, P. R., "Extension fo the Picewise Parabolic Method to Multidimensional Ideal Magnetohydrodynamics," *Journal of Computational Physics*, Vol. 115, No. 2, 1994, pp. 485–514. doi:10.1006/jcph.1994.1212

[19] Dai, W., and Woodward, P. R., "A Simple Finite Difference Scheme for Multidimensional Magnetohydrodynamic Equations," *Journal of Computational Physics*, Vol. 142, No. 2, 1998, pp. 331–369. doi:10.1006/jcph.1998.5944

[20] Balsara, D. S., and Spiecer, D. S., "A Staggered Mesh Algorithm Using High Order Gounov Fluxes to Ensure Solenoidal Magnetic Fields in Magnetohydroynamic Simulations," *Journal of Computational Physics*, Vol. 149, No. 2, 1999, pp. 270–292. doi:10.1006/jcph.1998.6153

[21] Toth, G., "The $\nabla \cdot \mathbf{B} = 0$ Constraint in Shock-Capturing Magneto-hydrodynamics," *Journal of Computational Physics*, Vol. 161, No. 2, 2000, pp. 605–652. doi:10.1006/jcph.2000.6519

[22] Jiang, B., Wu, J., and Povinelli, L. A., "The Origin of Spurious Solutions in Computational Electromagnetics," *Journal of Computational Physics*, Vol. 125, No. 1, 1996, pp. 104–123. doi:10.1006/jcph.1996.0082

[23] Brackbill, J. U., and Barnes, D. C., "The Effect of Nonzero Div B on the Numerical Solution of the Magnetohydrodynamic Equations," *Journal of Computational Physics*, Vol. 35, No. 3, 1980, pp. 426–429. doi:10.1016/0021-9991(80)90079-0

[24] Yee, K. S., "Numerical Solution of Initial Boundary Value Problems Involving Maxwell Equations in Isotropic Media," *IEEE Transactions on Antennas and Propagation*, Vol. 14, No. 3, 1966, pp. 302–307. doi:10.1109/TAP.1966.1138693

[25] Balsara, D. S., and Spiecer, D. S., "Maintaining Pressure Positivity in Magnetohydrodynamic Simulations," *Journal of Computational Physics*, Vol. 148, No. 1, 1999, pp. 133–148. doi:10.1006/jcph.1998.6108

[26] Balsara, D. S., "Divergence-Free Adaptive Mesh Refinement for Magnetohydrodynamics," *Journal of Computational Physics*, Vol. 174, No. 2, 2001, pp. 614–648. doi:10.1006/jcph.2001.6917

[27] Powell, K. G., "A Riemann Solver for Ideal MHD that Works in More than One Dimension," ICASE Report, 94-24, 1994.

[28] Powell, K. G., Roe, P. L., Linde, T. J., Gombosi, T. I., and De Zeeuw, D. L., "A Solution-Adaptive Upwind Scheme for Ideal Magnetohydrodynamics," *Journal of Computational Physics*, Vol. 154, No. 2, 1999, pp. 284–309. doi:10.1006/jcph.1999.6299

[29] Orszag, S. A., and Tang, C.-M., "Small-Scale Structure of Two-Dimensional Magnetohydrodynamic Turbulence," *Journal of Fluid Mechanics*, Vol. 90, No. 1, 1979, pp. 129–143. doi:10.1017/S002211207900210X

[30] Yee, H. C., and Sjogreen, B., "Efficient Low Dissipative High Order Schemes for Multiscale MHD Flows, II: Minimization of $\nabla \cdot \mathbf{B}$ Numerical Error," *Journal of Scientific Computing*, Vol. 29, No. 1, 2006, pp. 115–164. doi:10.1007/s10915-005-9004-5

[31] Roe, P. L., and Balsara, D. S., "Notes on the Eigensystem of Magnetohydrodynamics," *SIAM Journal on Applied Mathematics*, Vol. 56, No. 1, 1986, pp. 57–65.

[32] Cargo, P., and Gallice, G., "Roe Matrices for Ideal MHD and Systematic Construction of Roe Matrices for Systems of Conservation Laws," *Journal of Computational Physics*, Vol. 136, No. 2, 1997, pp. 446–466. doi:10.1006/jcph.1997.5773

[33] Jiang, G. S., and Wu, C. C., "A High-Order WENO Finite Difference Scheme for the Equations of Ideal Magnetohydrodynamics," *Journal of Computational Physics*, Vol. 150, No. 2, 1999, pp. 561–594. doi:10.1006/jcph.1999.6207

[34] Ekaterinaris, J. A., "High-Order Accurate, Low Numerical Diffusion Methods for Aerodynamics," *Progress in Aerospace Sciences*, Vol. 41, Nos. 3–4, 2005, pp. 192–300. doi:10.1016/j.paerosci.2005.03.003

[35] Balsara, D. S., and Shu, C-W., "Monotonicity Preserving Weighted Essentially Non-oscillatory Schemes with Increasingly High Order of Accuracy," *Journal of Computational Physics*, Vol. 160, No. 2, 2000, pp. 405–452. doi:10.1006/jcph.2000.6443

[36] Lee, D., and Deane, A. E., "An Unsplit Staggered Mesh Scheme for Multidimensional Magnetohydrodynamics," *Journal of Computational Physics*, Vol. 228, No. 4, 2009, pp. 952–975. doi:10.1016/j.jcp.2008.08.026

X. Zhong
Associate Editor